Effects of orbital composition in a pair of spin-orbit-split surface bands at Tl/Ge(111)

Philipp Eickholt,[1,*] Peter Krüger,[2] Sebastian D. Stolwijk,[1] Anke B. Schmidt,[1] and Markus Donath[1]
[1]*Physikalisches Institut, Westfälische Wilhelms-Universität Münster, Wilhelm-Klemm-Straße 10, 48149 Münster, Germany*
[2]*Institut für Festkörpertheorie, Westfälische Wilhelms-Universität Münster, Wilhelm-Klemm-Straße 10, 48149 Münster, Germany*
(Received 9 December 2015; published 8 February 2016)

The spin texture of the unoccupied surface electronic structure of the metal-semiconductor hybrid system Tl/Ge(111)-(1 × 1) is investigated by spin- and angle-resolved inverse photoemission as well as quasiparticle band-structure calculations. Spin-polarized surface bands with rotating spin and giant energy splitting are found along $\bar{\Gamma}\bar{K}(\bar{K}')$, forming valleys with alternating out-of-plane spin polarization at $\bar{K}$ and $\bar{K}'$. This behavior is known from the equivalent hybrid system on Si(111). Along $\bar{\Gamma}\bar{M}$, a pair of surface bands appears within a projected bulk band gap, whose equivalent on Tl/Si(111) is a surface resonance because, there, it overlaps with bulk states. Surprisingly, the spin splitting of these bands on Tl/Ge(111) is much smaller than on Tl/Si(111) despite the stronger surface localization and the heavier substrate. Our detailed analysis of the band structure and a tight-binding model including all relevant interactions show that a remarkable interplay between spin-orbit coupling and hybridization is responsible for this unexpected result. The comparison between the two similar hybrid systems demonstrates that the strength of the spin-orbit coupling alone, based on the atomic number of the respective elements, is not sufficient to estimate spin splittings of spin-orbit-influenced surface states.

DOI: 10.1103/PhysRevB.93.085412

I. INTRODUCTION

Spin-polarized electronic states can give rise to spin currents which are highly desirable for possible future spintronic applications. The lifting of inversion symmetry at the surface leads to spin-orbit-coupling (SOC) induced spin splitting of surface bands. For free-electron-like states on heavy-metal surfaces, such as Au(111) [1–3], the splitting has been described in terms of the Rashba-Bychkov model [4,5]. To integrate spintronic devices in today's silicon-based electronics, thin films of heavy metals with high SOC on semiconductor substrates are particularly interesting. Many of these metal-semiconductor hybrid systems [6–9] exhibit surface states with complex spin textures that go beyond the simple Rashba model due to the surface symmetry and hybridization effects. One example is the rotation of the spin-polarization vector of a spin-split surface state on the Tl/Si(111)-(1 × 1) surface, which has been observed for occupied and unoccupied states [10–12]. For the Tl-(1 × 1) structure on Ge(111), differences might be expected in view of the increased SOC of the heavier substrate and a weaker intralayer hybridization due to the larger lattice constant of germanium. While angle-resolved photoemission measurements [13–15] have shown that the occupied surface electronic structure of Tl/Ge(111) is very similar to Tl/Si(111), the question remains open for the unoccupied states. In addition, no spin-resolved measurements of the surface electronic structure, either occupied or unoccupied, have been reported so far.

We employed spin- and angle-resolved inverse photoemission and electronic-structure calculations to investigate the surface electronic structure of Tl/Ge(111)-(1 × 1). Along the high-symmetry direction $\bar{\Gamma}\bar{K}$, we identify a spin-split surface state with rotating spin-polarization vector and giant spin splitting very similar to Tl/Si(111)-(1 × 1). Surprisingly, the spin splitting of the surface state along $\bar{\Gamma}\bar{M}$ is found to be smaller for Tl/Ge(111) than for Tl/Si(111). This is counterintuitive in view of the larger SOC of the heavier substrate germanium and the fact that these states are resonant with Si bulk states for Tl/Si(111), while they reside in the bulk band gap for Tl/Ge(111). Consequently, they should be much more localized at the surface Tl atoms for Tl/Ge(111) and one might expect a larger spin-orbit-induced splitting, since SOC in these systems mainly results from the Tl atoms due to their large atomic number. We show that a remarkable combination of SOC and hybridization is responsible for the surprising differences in the spin splitting.

II. EXPERIMENTAL AND THEORETICAL METHODS

A. Experiment

The Ge(111) substrate (p doped) was cleaned by sputtering with 1 keV Ar^+ ions and subsequent annealing at 1120 K for 1 minute and 970 K for 10 minutes. After annealing, the $c(2 \times 8)$ surface reconstruction appeared in the low-energy electron diffraction (LEED) image. The surface quality was further verified with Auger electron spectroscopy. The Tl/Ge(111)-(1 × 1) overlayer system is a honeycomb layered structure with threefold symmetry ($p3m1$ space group) as depicted in the structural model in Fig. 1(a). It was prepared by evaporating one monolayer of Tl from a Ta crucible onto the clean Ge(111) substrate at 540 K. The LEED image in Fig. 1(b) shows a sharp diffraction pattern, indicating the (1 × 1) structure of the thallium overlayer.

The unoccupied electronic structure has been investigated with spin-resolved inverse photoemission (SR-IPE). Spin-polarized electrons (spin polarization 29%) from a GaAs photocathode are guided onto the sample at a defined angle of incidence θ. The transversal polarization direction can be chosen freely by mechanically rotating the electron source. Thus, the experiment is sensitive either to the in-plane spin-polarization direction perpendicular to $\mathbf{k}_\parallel$ (in-plane$_\perp$) or simultaneously to the out-of-plane spin component and the

*philippeickholt@uni-muenster.de

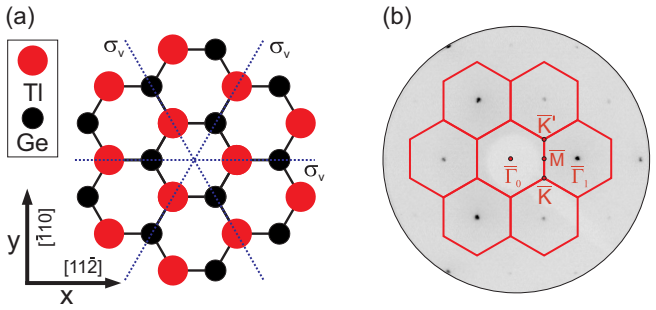

FIG. 1. (a) Structural model of the Tl/Ge(111)-(1 × 1) surface (top view). The vertical mirror planes σ_v are indicated by dashed lines. (b) LEED image ($E = 93$ eV) of Tl/Ge(111)-(1 × 1). The first and adjacent surface Brillouin zones with the respective high symmetry points are superimposed in red.

in-plane spin-polarization direction parallel to $\mathbf{k}_\parallel$ (in-plane$_\parallel$). Note that out-of-plane spin sensitivity is only obtained for $\theta \neq 0$. A detailed description is given in Ref. [16].

Electrons impinging on the surface may undergo optical transitions into energetically lower, unoccupied final states. In our setup, the emitted photons are detected at a fixed energy of 9.9 eV with a bandpass-type Geiger-Müller counter, where the acetone filling and the CaF_2 entrance window form the energy bandpass [17,18]. Spectra are obtained by varying the kinetic energy of the incident electrons, thereby probing final states of different energy. The total energy resolution of our experiment is 350 meV, while the angular resolution of the electron source is $\pm 1.5^\circ$. This corresponds to a k resolution of ± 0.03 Å^{-1} for an electronic state at the Fermi energy.

Spectra for the same θ, but with sensitivity to different spin-polarization directions have been measured consecutively. To ensure that in each case the same position in k-space is probed, we verified that the corresponding spin-integrated spectra match. Following the common procedure for spin-resolved measurements, spectra have been normalized to 100% spin polarization of the electron beam as described elsewhere [19].

B. Theory

We employ density-functional theory (DFT) with the local-density approximation [20] to obtain the ground-state properties of the system. The electronic wave functions are represented by Gaussian orbitals with s, p, and d symmetries [21]. Nonlocal norm-conserving pseudopotentials [22] that include scalar relativistic corrections and SOC are used in separable form [23]. The Tl/Ge(111) surface is described within the supercell approach. We use a slab consisting of a Tl adlayer, 70 Ge substrate layers, and a bottom H saturation layer. A vacuum layer of 12 Å is used to decouple neighboring slabs. We employ a Monkhorst-Pack (MP) mesh [24] of 10 × 10 × 1 for Brillouin zone integrations. The calculated bulk lattice constant is 5.62 Å. In structure optimization, the topmost eight layers were allowed to relax. For the energetically most favorable adsorption configuration, we obtain interlayer distances [25] at the surface in agreement with low-energy electron diffraction measurements and a former DFT calculation [13].

To obtain the quasiparticle band structure, we use the GW approximation [26] for the electron self-energy operator. We evaluate the one-body Green's function G and the screened Coulomb interaction W using LDA energies and wave functions. The frequency-dependence of the self-energy operator is treated by a plasmon-pole model and the nonlocal dielectric screening is described in a basis of plane waves [27]. SOC is fully taken into account in these calculations [28]. The GW calculations have been carried out for a supercell containing 18 Ge substrate layers and a 6 × 6 × 1 MP grid.

III. ENERGY DISPERSION AND SPIN TEXTURE OF SURFACE BANDS

To analyze the unoccupied electronic structure, SR-IPE spectra for various angles of electron incidence have been taken along $\bar{\Gamma}\bar{K}$ and $\bar{\Gamma}\bar{M}$. The energy dispersion of the surface states and their spin texture will be discussed in this section.

A. Results along $\bar{\Gamma}\bar{K}$

Figure 2 shows SR-IPE spectra for various angles of incidence θ along $\bar{\Gamma}\bar{K}$. Spectra in Fig. 2(a) are measured with sensitivity to the in-plane$_\perp$ spin-polarization direction (classical Rashba component). Figure 2(b) displays spectra with simultaneous sensitivity to the out-of-plane and in-plane$_\parallel$ spin-polarization directions. Since in our sample system the in-plane$_\parallel$ component is zero along $\bar{\Gamma}\bar{K}$ due to symmetry reasons, the spin dependence comes from the out-of-plane component alone [11]. As mentioned before, out-of-plane sensitivity is only available for $\theta \neq 0$. Therefore, the spectrum for $\theta = 0$ was not normalized to 100% spin polarization of the electron beam.

Six spectral features, labeled $S1$ to $S6$, are discernible in the spin-resolved spectra. $S1$ and $S2$ appear at $\bar{\Gamma}$ and are attributed to predominantly occupied surface states. They cross the Fermi energy in the vicinity of $\bar{\Gamma}$, as previously observed in photoemission studies [13,14]. The most prominent spectral features $S3$ and $S4$ correspond to a pair of spin-polarized surface states. For small θ, they are mainly in-plane$_\perp$ spin polarized. Upon approaching $\bar{K}$, the in-plane$_\perp$ spin polarization vanishes and the states becoming increasingly out-of-plane spin polarized. At $\bar{K}$, the states are fully out-of-plane spin polarized as a consequence of the prevailing C_3 symmetry [29]. Between $\bar{K}$ and $\bar{K}'$, the spin polarization is reversed (not shown).

The peak positions of the spectral features in Fig. 2 are translated into an $E(\mathbf{k}_\parallel)$ plot in Figs. 3(a) and 3(b). Colored triangles denote the different spin-polarization directions as schematically shown in the figure. Features without distinct spin polarization are symbolized as black squares. The calculated quasiparticle dispersion of the surface states is shown as black lines. Gray-shaded areas display the projected bulk band structure. The energy scale refers to the experimentally determined Fermi energy. To align the energetic positions of $S1$ and $S2$ at $\bar{\Gamma}$ in theory and experiment, the calculated bands have been shifted by 0.06 eV.

We find good agreement between the calculated and the experimentally determined dispersion of $S5$ and $S6$ and excellent agreement in the case of $S3$ and $S4$. Around $\bar{K}$, $S3$ and $S4$ exhibit a valley-like dispersion with a giant spin splitting

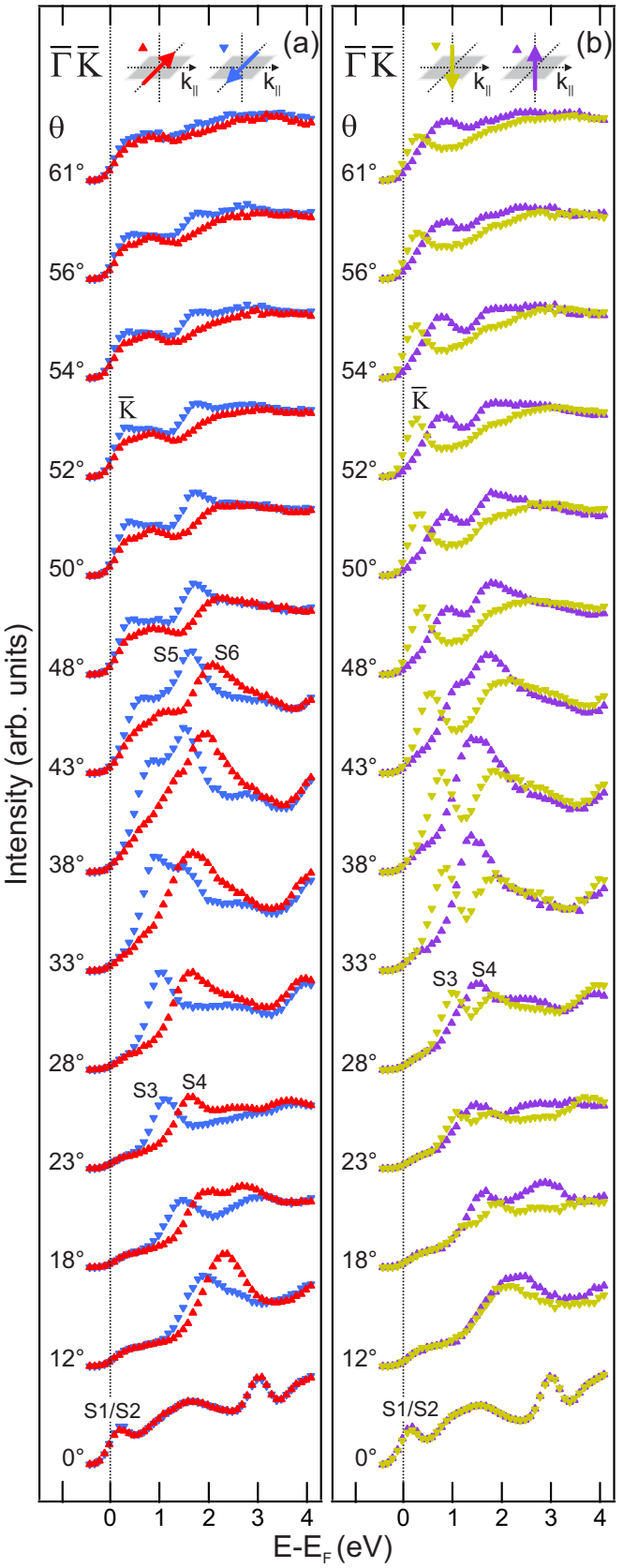

FIG. 2. SR-IPE spectra of Tl/Ge(111)-(1 × 1) along $\bar{\Gamma}\bar{K}$ with sensitivity to the (a) in-plane$_\perp$ and (b) out-of-plane spin-polarization directions. For $\theta = 52^\circ$, electronic states around the $\bar{K}$ point are probed. For larger θ, the spectral features belong to states along $\bar{K}\bar{M}$.

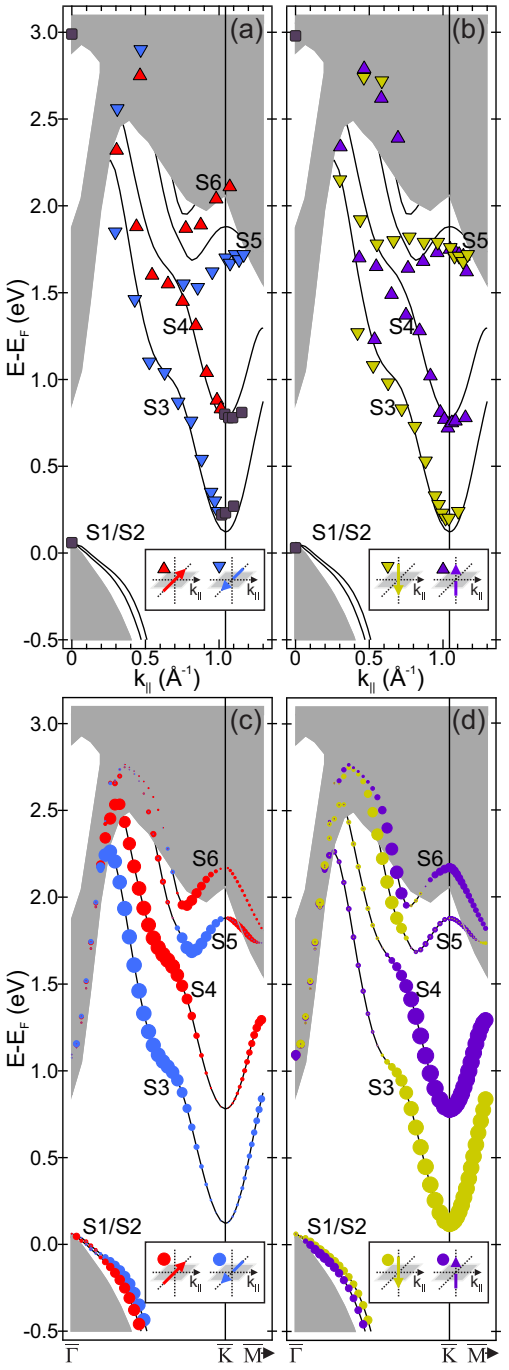

FIG. 3. (a),(b) $E(\mathbf{k}_\parallel)$ dispersion derived from the spectra in Figs. 2(a) and 2(b) with sensitivity to the (a) in-plane$_\perp$ and (b) out-of-plane spin-polarization directions. Black squares indicate features without distinct spin polarization. (c),(d) Quasiparticle band structures including SOC for the (c) in-plane$_\perp$ and (d) out-of-plane spin-polarization components. The gray-shaded area illustrates the projected bulk bands. The calculated dispersion of the surface states is plotted as solid lines, with the colored circles indicating the spin polarization. The areas of the circles are proportional to the spin polarization, with a maximum of 100%, e.g., for $S4$ at $\bar{K}$.

of about 0.5 eV at $\bar{K}$. Such fully spin-polarized valleys, when located at the Fermi energy, are very interesting in view of spin-polarized currents in future spintronic devices [30,31].

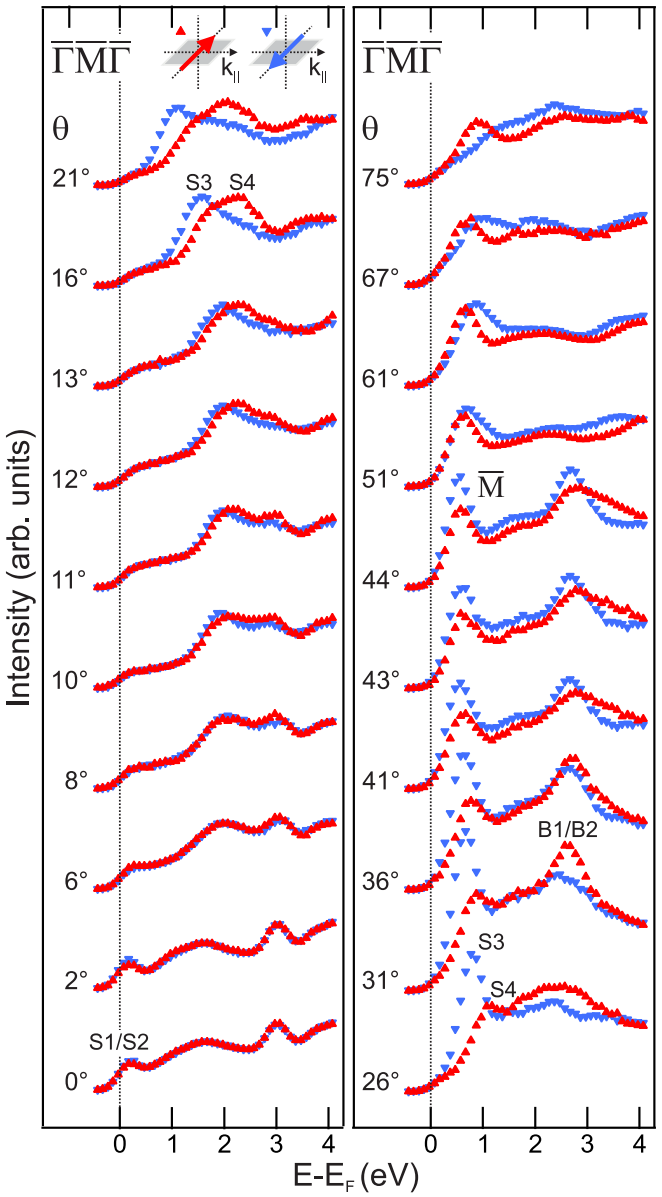

FIG. 4. SR-IPE spectra of Tl/Ge(111)-(1 × 1) along $\bar{\Gamma}\bar{M}\bar{\Gamma}$ with sensitivity to the in-plane$_\perp$ spin-polarization direction. For $\theta = 44°$, electronic states around the $\bar{M}$ point are probed. For larger θ, the spectral features belong to states in the second surface Brillouin zone.

B. Results along $\bar{\Gamma}\bar{M}\bar{\Gamma}$

Figure 4 shows SR-IPE spectra for various angles of incidence along $\bar{\Gamma}\bar{M}\bar{\Gamma}$ with sensitivity to the in-plane$_\perp$ spin-polarization direction. Any other spin-polarization direction is forbidden because $\bar{\Gamma}\bar{M}$ lies in a mirror plane [32]. The corresponding $E(\mathbf{k}_\parallel)$ plot is given in Fig. 5.

Again, we find a pair of spin-polarized surface states $S3$ and $S4$. In addition, we detect the already mentioned feature $S1$ and $S2$ and the bulk-derived features $B1$ and $B2$, which will not be discussed further. The dispersion of $S3$ and $S4$ is in excellent agreement with the results of the quasiparticle calculation, which predicts the states within an energy gap of the projected bulk band structure, i.e., as surface states. With respect to spin texture, $S3$ and $S4$ show an exclusive

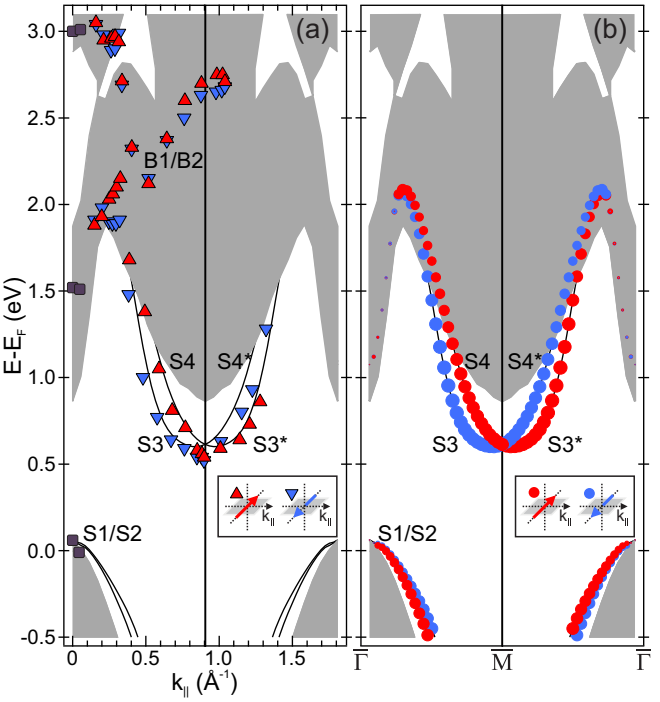

FIG. 5. (a) $E(\mathbf{k}_\parallel)$ dispersion derived from the spectra in Fig. 4. Black squares indicate features without distinct spin polarization. (b) Quasiparticle band structure including SOC for the in-plane polarization components. The gray-shaded area illustrates the projected bulk bands. The calculated dispersion of the surface states is plotted as solid lines, with the colored circles indicating the spin polarization. The areas of the circles are proportional to the spin polarization.

in-plane$_\perp$ spin polarization, changing sign when crossing the time-reversal invariant momentum (TRIM) point $\bar{M}$ ($\theta \approx 44°$) and entering the second surface Brillouin zone.

Summarizing, our results show that, in general, the electronic properties of Tl/Ge(111) and Tl/Si(111) are very similar: spin-polarized surface states with rotating spin and giant energy splitting along $\bar{\Gamma}\bar{K}$ and exclusive in-plane$_\perp$ spin polarization along $\bar{\Gamma}\bar{M}$. In detail, however, there exist noticeable differences in the band structures of the two systems. Close to the $\bar{M}$ point, the splitting between the states $S3$ and $S4$ is much larger for Tl/Si(111) than for Tl/Ge(111). We find a maximum energy splitting of only 0.4 eV at $k_\parallel = 0.50$ Å^{-1} for the Ge substrate compared with 0.65 eV at $k_\parallel = 0.56$ Å^{-1} for the Si substrate. This is counterintuitive at first glance, since these states are resonant with Si bulk states for Tl/Si(111), while they reside in the bulk band gap for Tl/Ge(111). In the following, however, we will show that a peculiar combination of SOC and hybridization gives rise to the astonishing differences in the spin splitting.

IV. UNRAVELING THE DISTINCT BEHAVIOR OF SURFACE BANDS AROUND $\bar{M}$

A. Probability density distribution

First, we consider the localization of $S3$ and $S4$ in real space for Tl/Ge(111) and Tl/Si(111), respectively. The panels on the left-hand side of Fig. 6 show the probability distribution

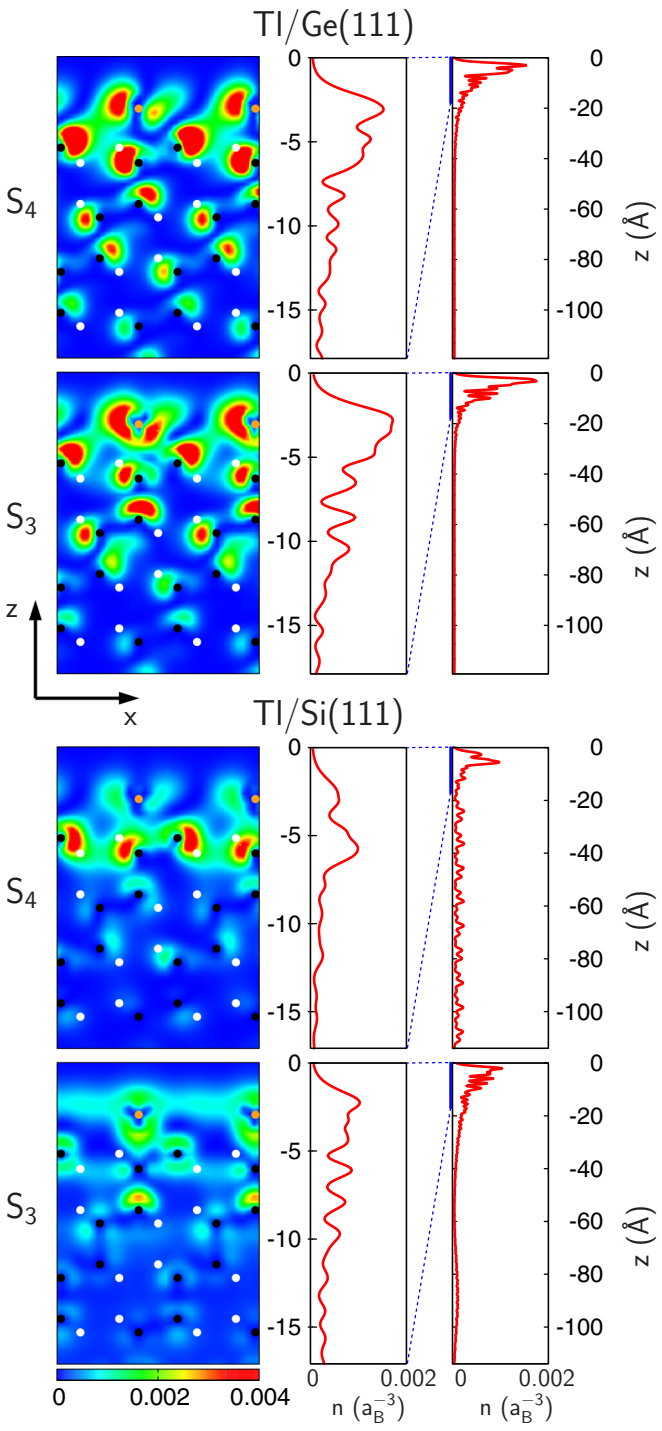

FIG. 6. Probability density distribution in the x-z plane of the surface states $S3$ and $S4$ at $\frac{3}{4}\bar{\Gamma}\bar{M}$ for Tl/Ge(111) (upper left panels) and Tl/Si(111) (lower left panels). Ge or Si atoms in the drawing plane are shown as black dots, otherwise as white dots. Orange dots represent Tl atoms. The z-dependent density distribution of each state integrated parallel to the surface is shown in the panels on the right side.

of these states in the x-z plane at $\frac{3}{4}\bar{\Gamma}\bar{M}$, where the splitting between $S3$ and $S4$ is particulary large. The z-dependent density distribution of each state integrated parallel to the surface is displayed on the right side of the panels. We notice the following features of the surface states.

(i) For both systems, the surface states are mainly localized at the topmost three surface layers but with distinctly larger amplitudes in the case of Tl/Ge(111).

(ii) In the bulk region, $S3$ and $S4$ decay exponentially for Tl/Ge(111) while they show an oscillating behavior for Tl/Si(111). These properties are correlated with the energetic position of the surface states: The former ones reside in the band gap while the latter ones overlap energetically with Si bulk states.

(iii) Most interestingly, in both systems there exist characteristic differences between $S3$ and $S4$. In the topmost layer, the probability density distribution of $S4$ is mainly formed by Tl p_x orbitals and has a node at the position of the Tl atoms, while the probability density of $S3$ has a substantial contribution of Tl p_z orbitals in this region. Obviously, this behavior is not in accord with the simple Rashba picture which assumes wave functions with the same orbital parts for a pair of spin-split states.

These results confirm our expectation that the probability density in the vicinity of the Tl nuclei is larger for Tl/Ge(111) in comparison to Tl/Si(111). They provide, however, no explanation of the observed difference in the spin splitting.

B. Band structure

For a deeper understanding of the $S3$, $S4$ spin splitting, we analyze the interplay of adsorbate and substrate states in Tl/Ge(111) and Tl/Si(111). To this end, we first switch off in our calculation the interaction between the Tl adlayer and the underlying substrate. The corresponding thallium DFT band structure (without SOC for simplicity) is shown in Figs. 7(a) and 7(b) together with the dangling-bond band and a characteristic surface resonance of the respective substrate. The Tl p_x and p_y orbitals are oriented parallel to the adlayer, and their strong overlap with those of neighboring atoms gives rise to the bands P_x^{Tl} and P_y^{Tl} with a large dispersion, while the interaction between neighboring Tl p_z orbitals induces the P_z^{Tl} bands which have smaller dispersions. The widths of the Tl-related bands are slightly larger for Tl/Si(111) in comparison to Tl/Ge(111) due to the smaller Si surface lattice constant and hence a stronger overlap of the orbitals.

The silicon and germanium substrates have [in their ideal (1×1) configuration] two characteristic features which turn out to be essential for the electronic properties of the adsorption systems. Firstly, there are dangling-bond bands P_z^{Ge} and P_z^{Si}, respectively, which mainly consist of p_z orbitals located at the atoms of the topmost surface layer. Note that P_z^{Si} has a slightly smaller dispersion and resides at $\bar{M}$ 0.34 eV higher [33] in energy than P_z^{Ge}. Secondly, at about 2 eV, both substrates show around $\bar{M}$ in the conduction bands surface resonances D^{Si} and D^{Ge}, respectively, which are formed by d orbitals.

To grasp the fundamental physics of the interaction between the Tl adlayer and the respective substrate, we consider in the next step simplified configurations of the interacting systems. These are modeled by supercells containing a Tl adlayer and only two layers of Ge or Si, respectively, as well as a H layer to saturate the dangling bonds at the lower surface. Figures 7(c) and 7(d) show the corresponding band structures including SOC. Around $\bar{K}$, there are almost no differences between the dispersions of $S3$ and $S4$ for both surfaces, while they distinctly differ around $\bar{\Gamma}$ and $\bar{M}$. For Tl/Si(111), in particular,

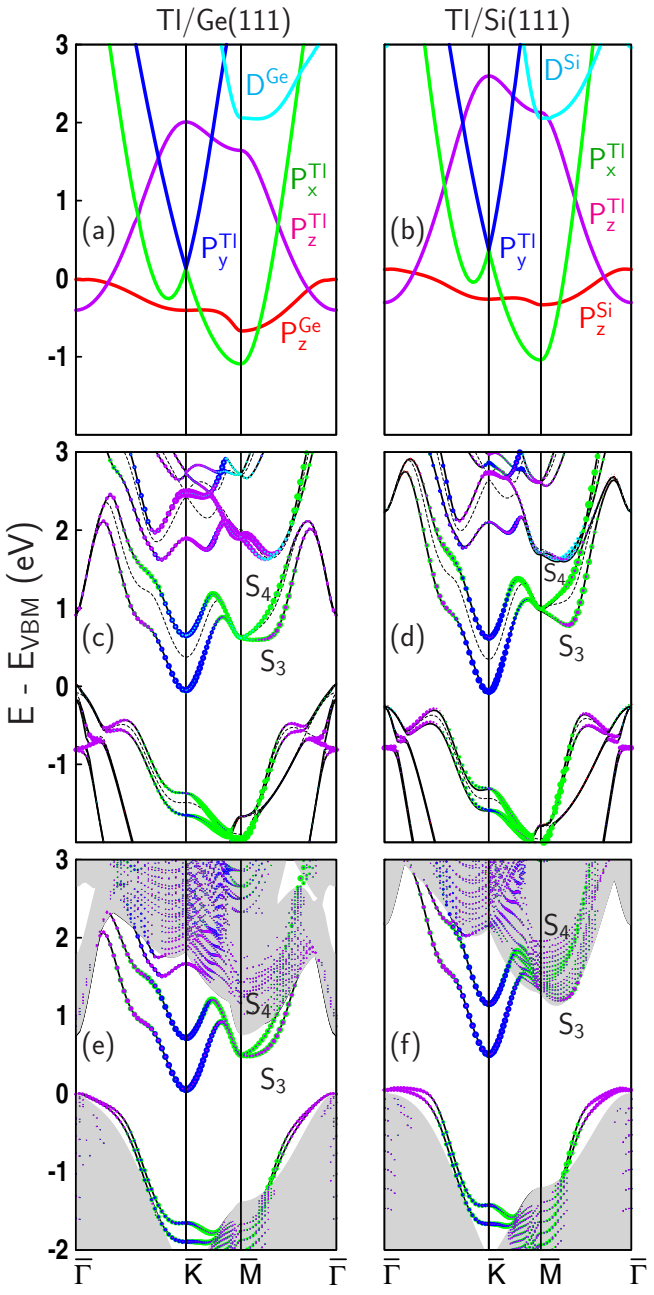

FIG. 7. DFT-LDA band structures for Tl/Ge(111) (left side) and Tl/Si(111) (right side). (a),(b) isolated Tl monolayer without SOC for the lattice constant of the respective substrate and dangling-bond bands P_z^{Ge}, P_z^{Si}, as well surface resonances D^{Ge}, D^{Si}. Interacting systems including SOC with (c),(d) two substrate layers and (e), (f) 70 substrate layers. The diameters of the green, blue, and magenta dots are proportional to the contributions of thallium P_x^{Tl}, P_y^{Tl}, and P_z^{Tl} orbitals of the respective states. The cyan dots in (c) and (d) depict the contributions of substrate d orbitals while contributions of substrate s and p orbitals are not indicated in (c)–(f). The dashed lines in (c) and (d) indicate the results of a calculation without SOC. A correction of the band gap has been applied in (e) and (f) according to quasiparticle calculations in this work and in Ref. [11].

we notice a strong downward dispersion of $S3$ from $\bar{M}$ to about $\frac{1}{4}\bar{M}\bar{\Gamma}$, and, concomitantly, a larger splitting between $S3$ and $S4$ than in the case of Tl/Ge(111). A Mulliken analysis [34] shows that $S3$ and $S4$ consist mainly of Tl p_x and p_y orbitals at $\bar{K}$, while Tl p_x and p_z as well as substrate dangling-bond orbitals contribute substantially to these states around $\bar{M}$. A comparison with the results of a calculation without SOC [dashed lines in Figs. 7(c) and 7(d)] reveals that SOC does not lead to an energetically uniform splitting of the former spin-degenerate bands in these systems. This is in particular the case for $S3$ and $S4$ around $\bar{M}$ where $S4$ deviates only slightly from the spin-degenerate band while $S3$ experiences a substantial $\mathbf{k}_\parallel$-dependent shift to lower energies.

The calculations with only two substrate layers exhibit already the essential features of the surface states, as can be inferred from a comparison with the results of computations employing supercells with 70 substrate layers as shown in Figs. 7(e) and 7(f). Around $\bar{K}$ and $\bar{M}$, in particular, there is good agreement between the respective sets of calculations for the dispersion of $S3$ and $S4$. However, there is an important point which is (naturally) not included in the calculations for the small supercells: Around $\bar{M}$, $S3$ and $S4$ are energetically resonant with Si bulk states for Tl/Si(111) while they reside in the band gap for Tl/Ge(111). The energetic broadening of the surface resonances is indicated by the cloud of small dots surrounding $S3$ and $S4$. The size of each dot exhibits the degree of spatial localization of the corresponding state at the Tl adlayer. Note that we have employed in Figs. 7(e) and 7(f) a scissors operator [35] to the DFT conduction bands to ease the comparison with experimental data and the results of our GW calculations in Figs. 3 and 5, as well as in Ref. [11].

The SOC induced by the Ge atoms has only a minor influence on the surface bands. Employing Ge pseudopotentials without SOC in our calculations (not shown here), we find that the splitting of $S3$ and $S4$ along $\bar{\Gamma}\bar{M}$ changes by less than 0.01 eV. This is unlike the situation in Bi/Ge(111) and Br/Ge(111), where the SOC of the Ge substrate induces a spin splitting of subsurface states extending deep into the bulk [15,36,37].

Summarizing, the calculations employing small as well as large supercells show, in accordance with our experimental findings, a distinctly larger splitting of $S3$ and $S4$ for Tl/Si(111) than for Tl/Ge(111). To shed light on the physical origin of this behavior, we simplify our treatment of these systems even more and consider in the next section a tight-binding (TB) model.

C. Tight-binding model

The formation of the surface states $S3$ and $S4$ along $\bar{M}\bar{\Gamma}$ (the k_x direction) can be understood on the basis of a tight-binding model [38] which comprises p_x^{Tl} and p_z^{Tl} orbitals at each atom of the thallium layer and p_z^{Ge} or p_z^{Si} orbitals modeling the dangling bond orbitals in the surface layer of the respective substrate. Exemplarily, we discuss here the case of Tl/Ge(111). We take the nearest-neighbor contributions for the Tl-Tl, Ge-Ge, and Tl-Ge interactions into account, and SOC λ between the thallium p orbitals is included in the on-site approximation [39]. Choosing the spin-quantization axis in the Rashba direction [the $\pm y$ direction as defined in Fig. 1 (a)], the interaction of states with antiparallel spin direction vanishes. For parallel spin, the resulting Hamiltonian matrices can be written in the basis $\{p_x^{\mathrm{Tl}}, p_z^{\mathrm{Tl}}, p_z^{\mathrm{Ge}}\}$

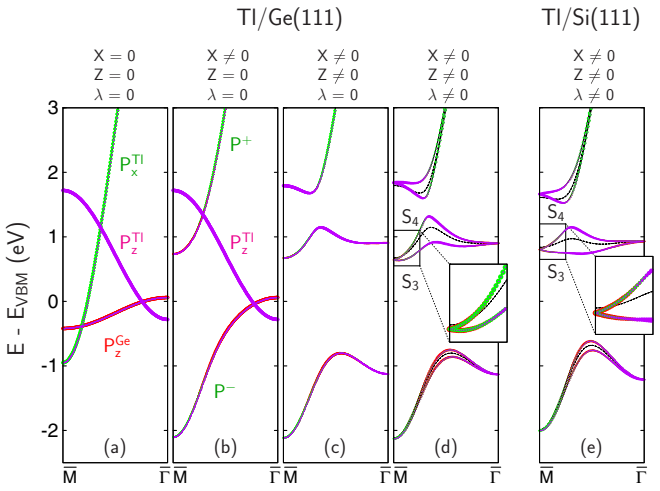

FIG. 8. Tight-binding model of the Tl/Ge(111) surface along $\bar{M}\bar{\Gamma}$ containing P_x^{Tl}, P_z^{Tl}, and P_z^{Ge} bands (a) without interaction, (b) with interaction between P_x^{Tl} and P_z^{Ge}, (c) with all interband interactions, and (d) with all interband and spin-orbit interactions. (e) The same model is applied to Tl/Si(111) with modified on-site energies for P_z^{Tl} and D_z^{Si}. For details see text. The diameters of the green, magenta, and red dots are proportional to the contributions of thallium P_x^{Tl}, P_z^{Tl}, and substrate P_z^{Ge} orbitals of the respective states. The dashed lines in (d) and (e) indicate the results of a calculation without SOC.

along k_x ($\bar{M}\bar{\Gamma}$) as

$$H^{\uparrow} = \begin{pmatrix} H_{xx}^{\mathrm{Tl}} & +i\lambda & X \\ -i\lambda & H_{zz}^{\mathrm{Tl}} & Z \\ X^* & Z^* & H_{zz}^{\mathrm{Ge}} \end{pmatrix}, \; H^{\downarrow} = \begin{pmatrix} H_{xx}^{\mathrm{Tl}} & -i\lambda & X \\ +i\lambda & H_{zz}^{\mathrm{Tl}} & Z \\ X^* & Z^* & H_{zz}^{\mathrm{Ge}} \end{pmatrix}. \tag{1}$$

All matrix elements depend on TB parameters chosen on the basis of our DFT calculations and, except for the SOC parameter λ, are k_x dependent. The main diagonal consists of the respective intraband interactions H_{xx}^{Tl}, H_{zz}^{Tl}, and H_{zz}^{Ge} for a hexagonal lattice. In the minor diagonal we find the interband interaction X (Z) between the thallium p_x^{Tl} (p_z^{Tl}) and germanium p_z^{Ge} orbitals. No interaction between p_x^{Tl} and p_z^{Tl} orbitals occurs since the corresponding integrals are zero. The spin-orbit interaction enters with opposite sign in the Hamilton matrices for spin-up and spin-down electrons, respectively.

Figure 8 shows the eigenvalues of the Hamilton matrices for different interactions X, Z, and λ. Neglecting all couplings, the eigenvalues depicted in Fig. 8(a) represent the band structure of an isolated Tl adlayer without SOC and the dangling-bond band of an ideal Ge(111) surface in accord with the DFT result plotted in the rightmost part of Fig. 7(a) along $\bar{M}\bar{\Gamma}$. The interaction X induces a strong rearrangement of the bands P_x^{Tl} and P_z^{Ge} and opens a hybridization gap as shown in Fig. 8(b). Close to $\bar{M}$, the newly formed states P_+ and P_- consist of both p_x^{Tl} and p_z^{Ge} orbitals.

Considering the interaction Z in addition to X, a gap opens between P_- and P_z^{Tl}, as well as between P_+ and P_z^{Tl} [see Fig. 8(c)]. The latter one arises due to the interaction between the p_z^{Tl} orbitals and the p_z^{Ge} components of P_+.

Eventually, the spin-orbit interaction λ induces a splitting of the spin-degenerate states as shown in Fig. 8(d). The resulting states $S3$ and $S4$ are spin polarized with a spin orientation in $+y$ and $-y$ directions, respectively. The dispersions of these states are not symmetric with respect to the former unpolarized state [Fig. 7(c) and dashed-dotted line in Fig. 8(d)], since the effective interaction resulting from SOC λ and the hybridization strength Z sum up for the $S3$ spin-up electrons while they compensate in parts for the $S4$ spin-down electrons [38]. Concomitantly, this leads to a stronger mixing of p_z^{Tl} orbitals into $S3$ than into $S4$.

Between $\bar{M}$ and $\frac{1}{2}\bar{M}\bar{\Gamma}$, the TB model describes the dispersion and the orbital composition of the surface states, in good agreement with the results of our DFT calculation for Tl/Ge(111) [see Figs. 7(c) and 7(e)]. Beyond $\frac{1}{2}\bar{M}\bar{\Gamma}$, however, the agreement becomes increasingly less since the influence of further substrate states, which are not included in the TB model, is more important close to $\bar{\Gamma}$.

Next, we apply the TB model to Tl/Si(111). From our DFT results for the isolated Tl layer and the clean substrate surfaces in Figs. 7(a) and 7(b) we know that (i) the Si dangling-bond band with its smaller dispersion resides at $\bar{M}$ 0.34 eV higher in energy than the corresponding band at Ge(111), and (ii) a d-like surface resonance at the Si(111) surface is at $\bar{M}$ slightly lower in energy than the thallium P_z^{Tl} band, while they are distinctly separated in energy for Ge(111). Due to the interaction between Tl p_z orbitals and substrate d orbitals, the P_z^{Tl} state resides eventually 0.23 eV lower in energy for Tl/Si(111) than for Tl/Ge(111), as depicted in Figs. 7(c) and 7(d). We put this information into our TB model by (i) changing the on-site energy and intraband TB parameter for the P_z^{Si} band accordingly, and (ii) employing a downward shift of -0.23 eV for the P_z^{Tl} band in order to consider approximately the effect of the substrate d-like resonance [40].

We do not modify any other model parameter, and we obtain the band structure shown in Fig. 8(e). A larger spin splitting between $S3$ and $S4$ with respect to Tl/Ge(111) occurs, remarkably, without changing the SOC parameter $\lambda = 0.3$ eV or any thallium-substrate interaction parameter. In this way, the model describes the characteristic differences between Tl/Ge(111) and Tl/Si(111) with respect to the surface states $S3$ and $S4$. Summarizing, the smaller energetic difference between P^+ and P_z^{Tl} for Tl/Si(111) in comparison with Tl/Ge(111) gives rise to a larger splitting of the surface states. The same line of reasoning applies for the results of our *ab initio* calculations. Here, the thallium P_z^{Tl} band appears as a broad resonance which is energetically closer to $S4$ for Tl/Si(111) in comparison with Tl/Ge(111), as shown in Figs. 7(e) and 7(f).

V. CONCLUSION

We present spin-resolved inverse-photoemission measurements of the unoccupied electronic structure of Tl/Ge(111)-(1 × 1) along the high-symmetry directions $\bar{\Gamma}\bar{K}$ and $\bar{\Gamma}\bar{M}$. Our experimental results agree excellently with our quasiparticle band structures. Around $\bar{K}$, we find surface states with a valley-like dispersion and full out-of-plane spin polarization, spin split in energy by 0.5 eV and very similar to Tl/Si(111)-(1 × 1) [11]. Unlike on Tl/Si(111), where surface resonances appear around the $\bar{M}$ point, the corresponding states on Tl/Ge(111) reside in a band gap. Despite the surface-state character and the larger SOC of the germanium

substrate, surprisingly, the spin splitting of the surface states around $\bar{M}$ is significantly smaller on Tl/Ge(111) than on Tl/Si(111). We disentangled the interactions contributing to the spin splitting of the surface states with the help of a tight-binding model. Thus, we could trace back the effect to a peculiar mixture of SOC and hybridization, demonstrating that a direct "translation" of SOC size into a spin splitting is not possible in such complex metal-semiconductor hybrid systems. Contrasting Tl/Ge(111) directly with Tl/Si(111) nicely illustrates the negligible role of the substrate SOC in comparison with hybridization effects.

ACKNOWLEDGMENTS

We thank Kazuyuki Sakamoto for his assistance with the sample and the Tl-film preparation. Financial support by the Deutsche Forschungsgemeinschaft (DFG) is gratefully acknowledged.

[1] S. LaShell, B. A. McDougall, and E. Jensen, Phys. Rev. Lett. **77**, 3419 (1996).
[2] M. Hoesch, M. Muntwiler, V. N. Petrov, M. Hengsberger, L. Patthey, M. Shi, M. Falub, T. Greber, and J. Osterwalder, Phys. Rev. B **69**, 241401(R) (2004).
[3] S. N. P. Wissing, C. Eibl, A. Zumbülte, A. B. Schmidt, J. Braun, J. Minár, H. Ebert, and M. Donath, New J. Phys. **15**, 105001 (2013).
[4] Yu. A. Bychkov and É. I. Rashba, JETP Lett. **39**, 78 (1984).
[5] For a recent discussion concerning the physical origin of the spin splitting in Au(111), see, e.g., Refs. [41,42].
[6] J. Ibanez-Azpiroz, A. Eiguren, and A. Bergara, Phys. Rev. B **84**, 125435 (2011).
[7] A. Takayama, T. Sato, S. Souma, and T. Takahashi, Phys. Rev. Lett. **106**, 166401 (2011).
[8] P. Höpfner, J. Schäfer, A. Fleszar, J. H. Dil, B. Slomski, F. Meier, C. Loho, C. Blumenstein, L. Patthey, W. Hanke, and R. Claessen, Phys. Rev. Lett. **108**, 186801 (2012).
[9] K. Sakamoto, T. H. Kim, T. Kuzumaki, B. Müller, Y. Y., M. Ohtak, J. R. Osiecki, K. Miyamoto, Y. Takeichi, A. Harasawa, S. D. Stolwijk, A. B. Schmidt, J. Fujii, R. I. G. Uhrberg, M. Donath, H. W. Yeom, and T. Oda, Nat. Commun. **4**, 2073 (2013).
[10] K. Sakamoto, T. Oda, A. Kimura, K. Miyamoto, M. Tsujikawa, A. Imai, N. Ueno, H. Namatame, M. Taniguchi, P. E. J. Eriksson, and R. I. G. Uhrberg, Phys. Rev. Lett. **102**, 096805 (2009).
[11] S. D. Stolwijk, A. B. Schmidt, M. Donath, K. Sakamoto, and P. Krüger, Phys. Rev. Lett. **111**, 176402 (2013).
[12] S. D. Stolwijk, K. Sakamoto, A. B. Schmidt, P. Krüger, and M. Donath, Phys. Rev. B **91**, 245420 (2015).
[13] S. Hatta, C. Kato, N. Tsuboi, S. Takahashi, H. Okuyama, T. Aruga, A. Harasawa, T. Okuda, and T. Kinoshita, Phys. Rev. B **76**, 075427 (2007).
[14] Y. Ohtsubo, S. Hatta, H. Okuyama, and T. Aruga, J. Phys. Condens. Matter **24**, 092001 (2012).
[15] T. Aruga, J. Electron Spectrosc. Relat. Phenom. **201**, 74 (2015).
[16] S. D. Stolwijk, H. Wortelen, A. B. Schmidt, and M. Donath, Rev. Sci. Instrum. **85**, 013306 (2014).
[17] D. Funnemann and H. Merz, J. Phys. E **19**, 554 (1986).
[18] M. Budke, V. Renken, H. Liebl, G. Rangelov, and M. Donath, Rev. Sci. Instrum. **78**, 083903 (2007).
[19] M. Donath, Surf. Sci. Rep. **20**, 251 (1994).
[20] J. P. Perdew and A. Zunger, Phys. Rev. B **23**, 5048 (1981).
[21] We use linear combinations of Gaussian orbitals [43,44] with different decay constants, which have been determined by minimalization of the total energy. We employ decay constants of 0.10, 0.51, 0.75, and 0.97 for thallium, 0.19 and 0.50 for Ge, and 0.19 and 0.56 for Si. To better account for the spatial extent of the wave functions at the surface, we use three shells with decay constants of 0.12, 0.40, and 0.56 for the topmost Ge and Si atoms. All decay constants are given in atomic units.
[22] D. R. Hamann, Phys. Rev. B **40**, 2980 (1989).
[23] L. A. Hemstreet, C. Y. Fong, and J. S. Nelson, Phys. Rev. B **47**, 4238 (1993).
[24] H. J. Monkhorst and J. D. Pack, Phys. Rev. B **13**, 5188 (1976).
[25] The interlayer distance between Tl and Ge is 2.19 Å and the distances between the adjacent Ge layers are 0.97, 2.44, 0.81, 2.45, and 0.82 Å, respectively.
[26] M. S. Hybertsen and S. G. Louie, Phys. Rev. B **34**, 5390 (1986).
[27] C. Sommer, P. Krüger, and J. Pollmann, Phys. Rev. B **85**, 165119 (2012).
[28] T. Förster, P. Krüger, and M. Rohlfing, Phys. Rev. B **92**, 201404 (2015).
[29] T. Oguchi and T. Shishidou, J. Phys. Condens. Matter **21**, 092001 (2009).
[30] S. Datta and B. Das, Appl. Phys. Lett. **56**, 665 (1990).
[31] R. Jansen, Nat. Mater. **11**, 400 (2012).
[32] S. D. Stolwijk, K. Sakamoto, A. B. Schmidt, P. Krüger, and M. Donath, Phys. Rev. B **90**, 161109(R) (2014).
[33] The relative positions of the Tl adlayer bands and the substrate bands have been inferred from DFT calculations employing supercells with a large distance of 8 Å between the adlayer and the respective substrate.
[34] R. S. Mulliken, J. Chem. Phys. **23**, 1833 (1955).
[35] Scissors shifts of 0.36 eV for Ge and 0.66 eV for Si were used.
[36] Y. Ohtsubo, S. Hatta, K. Yaji, H. Okuyama, K. Miyamoto, T. Okuda, A. Kimura, H. Namatame, M. Taniguchi, and T. Aruga, Phys. Rev. B **82**, 201307(R) (2010).
[37] Y. Ohtsubo, S. Hatta, N. Kawai, A. Mori, Y. Takeichi, K. Yaji, H. Okuyama, and T. Aruga, Phys. Rev. B **86**, 165325 (2012).
[38] S. N. P. Wissing, K. T. Ritter, P. Krüger, A. B. Schmidt, and M. Donath, Phys. Rev. B **91**, 201403(R) (2015).
[39] M. D. Jones and R. C. Albers, Phys. Rev. B **79**, 045107 (2009).
[40] For simplicity, d orbitals are not included explicitly in the TB model.
[41] E. E. Krasovskii, Phys. Rev. B **90**, 115434 (2014).
[42] H. Ishida, Phys. Rev. B **90**, 235422 (2014).
[43] W. Lu, P. Krüger, and J. Pollmann, Phys. Rev. B **60**, 2495 (1999).
[44] J. Wieferink, P. Krüger, and J. Pollmann, Phys. Rev. B **74**, 205311 (2006).